

Heat capacity of low density neutron matter: from quantum to classical regimes

A. Pastore^{1*}, N. Chamel¹ and J. Margueron²

¹*Institut d’Astronomie et d’Astrophysique, CP 226, Université Libre de Bruxelles, B-1050 Bruxelles, Belgium*

²*Université de Lyon, F-69003 Lyon, France; Université Lyon 1, 43 Bd. du 11 Novembre 1918, F-69622 Villeurbanne cedex, France
CNRS-IN2P3, UMR 5822, Institut de Physique Nucléaire de Lyon*

11 June 2021

ABSTRACT

The heat capacity of neutron matter is studied over the range of densities and temperatures prevailing in neutron-star crusts, allowing for the transition to a superfluid phase at temperatures below some critical temperature T_{sf} and including the transition to the classical limit. Finite temperature Hartree-Fock-Bogoliubov equations (FTHFB) are solved and compared to existing approximate expressions. In particular, the formula given by Levenfish and Yakovlev is found to reproduce the numerical results with a high degree of accuracy for temperatures $T \leq T_{sf}$. In the non-superfluid phase, $T \geq T_{sf}$, the linear approximation is valid only at temperature $T \ll T_{Fn}$ (T_{Fn} being the Fermi temperature of the neutron gas) which is rarely the case in the shallow layers of the neutron star’s crust. A non-perturbative interpolation between the quantal and the classical regimes is proposed here. The heat capacity, conveniently parametrized solely in terms of T_{sf} , T_{Fn} , and the neutron number density n_n , can be easily implemented in neutron-star cooling simulations.

Key words: neutron star crust – heat capacity – neutron matter – superfluidity

* E-mail: apastore@ulb.ac.be

1 INTRODUCTION

Neutron stars (NSs) are formed from the catastrophic gravitational core collapse of stars with a mass $M > 8M_{\odot}$ (Haensel et al. 2007). During the first tens of seconds after the collapse, the newly formed proto-neutron star with a radius of about 50 km stays very hot with internal temperatures of the order of $\sim 10^{11} - 10^{12}$ K. But it rapidly cools down and shrinks into an ordinary neutron star by emitting neutrinos. As the temperature drops, the outer layers of the star crystallize into a solid crust, whose innermost region is permeated by “free” neutrons (see Chamel & Haensel 2008, for a review of neutron-star crusts). At temperatures T lower than the Fermi temperature T_{Fn} , the neutron liquid becomes degenerate. As the temperature reaches some critical temperature T_{sf} , the neutron liquid undergoes a transition to a spin-singlet superfluid phase by forming Cooper pairs, like electrons in conventional superconductors. Due to its relatively low neutrino emissivity, the crust of a newly-born neutron star cools less rapidly than the core and thus stays hotter. As a result, the surface temperature decreases slowly during the first ten to hundred years and then suddenly drops when the *cooling wave* from the core reaches the surface. The evolution of the surface temperature of a young neutron star thus depends essentially on the thermal properties of its crust (Lattimer et al. 1994; Gnedin et al. 2001).

While the cooling of very young neutron stars has not been observed yet, the thermal relaxation of neutron-star crusts has been recently monitored in a few quasi-persistent soft X-ray transients (see Page & Reddy 2012, for a recent review). In these binary systems, usually called Low-Mass X-Ray Transients (LMXRT), a neutron star accretes matter from a companion star during several years or decades, driving the neutron-star crust out of its thermal equilibrium with the core. After the accretion stops, the heated crust relaxes towards equilibrium. While the thermal relaxation of young isolated NSs is mostly governed by the thermal properties of the densest layers of the NS crust, the thermal relaxation of LMXRT is expected to be very sensitive to the thermal properties of the shallower layers of the crust, especially near the transition between the inner and the outer crusts (Page & Reddy 2012). In this region of the NS crust, T may be not only higher than T_{sf} but also to T_{Fn} so that neutrons can be treated as a classical gas: their heat capacity does not increase linearly with T as in the deeper

arXiv:1501.03364v1 [astro-ph.SR] 14 Jan 2015

crustal regions where $T_{sf} \leq T \ll T_{Fn}$, but becomes essentially independent of T . Assuming that neutrons are degenerate in all regions of the crust may thus considerably overestimate the crustal heat capacity hence also the thermal relaxation time of LMXRT.

In this paper, we study the neutron contribution to the heat capacity of the neutron-star crust focusing on the region close to the neutron drip transition. Although the presence of inhomogeneities may alter the neutron heat capacity (see, e.g., Margueron & Sandulescu 2012), we shall simply consider here that the neutron liquid is homogeneous, as generally assumed in neutron-star cooling simulations (see, e.g., Page & Reddy 2012). Over the past years, the properties of dilute neutron matter have been extensively studied. Microscopic calculations based on realistic nucleon-nucleon potentials and following different many-body approaches tend to yield similar results, at least at low enough densities (Baldo & Burgio 2012). On the other hand, most of these calculations have been restricted to $T = 0$, and therefore they cannot be directly applied to neutron-star cooling simulations. For this reason, we have employed the finite-temperature Hartree-Fock-Bogoliubov (FTHFB) method, which is briefly reviewed in Section 2. The neutron heat capacity is studied in Section 3 for both the classical and degenerate regimes.

2 FINITE-TEMPERATURE HARTREE-FOCK-BOGOLIUBOV METHOD

The neutron pairing phenomenon is studied here using the self-consistent finite-temperature Hartree-Fock-Bogoliubov (FTHFB) method with effective nucleon-nucleon interactions (Goodman 1981; Sandulescu 2004; Margueron & Sandulescu 2012; Pastore 2012). This method not only provides a convenient parametrization of microscopic neutron-matter calculations based on realistic potentials at $T = 0$, but can also be applied to determine in a consistent way the properties of neutron matter at finite temperatures including the transition between the quantum and classical regimes. Moreover, the same method can also be applied to study inhomogeneous nuclear matter like neutron-star crusts (see, e.g., Margueron & Sandulescu 2012).

A key quantity for characterizing the superfluid phase is the pairing gap function $\Delta_n(k)$, k being the wave vector. This function, which is related to the binding energy of a pair, depends also on the temperature T (Δ_n vanishing at $T \geq T_{sf}$) and on the neutron number density n_n . The pairing gap can be determined by solving the following equations (the units used throughout this paper are such that the Boltzmann constant is $k_B = 1$):

$$\Delta_n(k) = -\frac{1}{4} \int \frac{d^3 k'}{(2\pi)^3} v(k, k') \frac{\Delta_n(k')}{E_n(k')} \tanh\left(\frac{E_n(k')}{2T}\right), \quad (1)$$

$$n_n = \int \frac{d^3 k'}{(2\pi)^3} \left[1 - \frac{\varepsilon_n(k') - \mu_n}{E_n(k')} \tanh\left(\frac{E_n(k')}{2T}\right) \right], \quad (2)$$

where $\varepsilon_n(k)$ denotes the neutron single-particle energies, $E_n(k) = \sqrt{(\varepsilon_n(k) - \mu_n)^2 + \Delta_n(k)^2}$ the neutron quasi-particle energies, μ_n the neutron chemical potential, and $v(k, k')$ the matrix elements of the effective pairing interaction. As in conventional superconductors, the effective pairing interaction may not necessarily be the same as the effective interaction which determines the single-particle properties in dense matter. For the latter, we use a zero-range effective interaction of the Skyrme type (Skyrme 1958; Bender et al. 2003)

$$\begin{aligned} v(\mathbf{r}_i, \mathbf{r}_j) = & t_0(1 + x_0 P_\sigma) \delta(\mathbf{r}_{ij}) + \frac{1}{2} t_1(1 + x_1 P_\sigma) \frac{1}{\hbar^2} [p_{ij}^2 \delta(\mathbf{r}_{ij}) + \delta(\mathbf{r}_{ij}) p_{ij}^2] + t_2(1 + x_2 P_\sigma) \frac{1}{\hbar^2} \mathbf{p}_{ij} \cdot \delta(\mathbf{r}_{ij}) \mathbf{p}_{ij} \\ & + \frac{1}{6} t_3(1 + x_3 P_\sigma) n_n(\mathbf{r})^\alpha \delta(\mathbf{r}_{ij}) + \frac{i}{\hbar^2} W_0(\hat{\boldsymbol{\sigma}}_i + \hat{\boldsymbol{\sigma}}_j) \cdot \mathbf{p}_{ij} \times \delta(\mathbf{r}_{ij}) \mathbf{p}_{ij} \quad , \end{aligned} \quad (3)$$

where $\mathbf{r}_{ij} = \mathbf{r}_i - \mathbf{r}_j$, $\mathbf{r} = (\mathbf{r}_i + \mathbf{r}_j)/2$, $\mathbf{p}_{ij} = -i\hbar(\nabla_i - \nabla_j)/2$ is the relative momentum, $\hat{\boldsymbol{\sigma}}_i$ and $\hat{\boldsymbol{\sigma}}_j$ are Pauli spin matrices, and P_σ is the two-body spin-exchange operator. Skyrme effective interactions were shown to be well suited for reproducing microscopic calculations at both zero and finite temperatures (Fantina et al. 2012). Using Eq. (3), the neutron single-particle energies can be expressed as

$$\varepsilon_n(k) = \frac{\hbar^2 k^2}{2m_n^*} + U_n, \quad (4)$$

where U_n denotes the (self-consistent) mean potential field felt by neutrons whereas m_n^* is the (self-consistent) mean neutron effective mass given by (Bender et al. 2003)

$$\frac{\hbar^2}{2m_n^*} = \frac{\hbar^2}{2m_n} + \frac{1}{8} [t_1(1 - x_1) + 3t_2(1 + x_2)] n_n, \quad (5)$$

m_n being the ‘‘bare’’ neutron mass. Since the FTHFB equations (1)-(2) depend only on the difference $\varepsilon_n(k) - \mu_n$, the pairing gap function is actually independent of the potential U_n . It is therefore convenient to introduce a shifted chemical potential $\nu_n \equiv \mu_n - U_n$. In this way, we have $\varepsilon_n(k) - \mu_n = \epsilon_n(k) - \nu_n$ with

$$\epsilon_n(k) = \frac{\hbar^2 k^2}{2m_n^*}, \quad (6)$$

so that U_n disappears from the FTHFB equations.

As for pairing, we shall also consider zero-range effective interaction of the form

$$v(\mathbf{r}_i, \mathbf{r}_j) = v^\pi(n_n(\mathbf{r}))\delta(\mathbf{r}_{ij}) \quad . \quad (7)$$

In this case, the matrix elements of the pairing interaction reduce to $v(k, k') = v^\pi(n_n)$. It can thus be seen from Eq. (1) that the pairing gap function is independent of \mathbf{k} . As shown by Chamel (2010), the pairing strength $v^\pi(n_n)$ can be directly inferred from microscopic calculations of the pairing gap function $\Delta_n(n_n)$ at $T = 0$ as follows

$$v^\pi(n_n) = -\frac{8\pi^2}{\sqrt{\nu_n}} \left(\frac{\hbar^2}{2m_n^*} \right)^{3/2} \left[2 \log \left(\frac{2\nu_n}{\Delta_n} \right) + \Lambda \left(\frac{\varepsilon_\Lambda}{\nu_n} \right) \right]^{-1} \quad (8)$$

with

$$\Lambda(x) = \log(16x) + 2\sqrt{1+x} - 2 \log(1 + \sqrt{1+x}) - 4. \quad (9)$$

The only free parameter is the pairing cutoff ε_Λ which needs to be introduced to regularize divergences in Eq. (1) arising from the zero-range of the interaction. The pairing functional defined in this way ensures that the solution of the FTHFB equations (1)-(2) coincides exactly with Δ_n at $T = 0$. With the effective interactions considered here, the gap equations (1) and (2) for $T < T_{sf}$ reduce to

$$1 = -\frac{1}{8} v^\pi(n_n) \int_{-\infty}^{\nu_n + \varepsilon_\Lambda} d\epsilon \frac{D(\epsilon)}{E(\epsilon)} \tanh \left(\frac{E(\epsilon)}{2T} \right), \quad (10)$$

$$n_n = \int_{-\infty}^{+\infty} d\epsilon D(\epsilon) \left[1 - \frac{\epsilon - \nu_n}{E(\epsilon)} \tanh \left(\frac{E(\epsilon)}{2T} \right) \right], \quad (11)$$

where $E(\epsilon) = \sqrt{\Delta_n^2 + (\epsilon - \nu_n)^2}$, and $D(\epsilon)$ denotes the density of neutron single-particle states, defined as

$$D(\epsilon) = 2 \int \frac{d^3k}{(2\pi)^3} \delta(\epsilon - \epsilon_n(k)) = \frac{1}{2\pi^2} \left(\frac{2m_n^*}{\hbar^2} \right)^{3/2} \sqrt{\epsilon}. \quad (12)$$

3 HEAT CAPACITY OF DILUTE NEUTRON MATTER

The neutron heat capacity C_V^n (per unit volume) is defined by (Landau & Lifchitz 1980a)

$$C_V^n(n_n, T) = T \left. \frac{\partial S^n}{\partial T} \right|_{n_n}, \quad (13)$$

where S^n is the entropy density given by

$$S^n(n_n, T) = - \int d\epsilon [f(\epsilon) \log f(\epsilon) + (1 - f(\epsilon)) \log(1 - f(\epsilon))], \quad (14)$$

with $f(\epsilon) = (1 + \exp(E(\epsilon)/T))^{-1}$. Injecting Eq. (14) into (13) yields the general expression

$$C_V^n(n_n, T) = \int d\epsilon (1 - f(\epsilon)) f(\epsilon) \left[\left(\frac{E(\epsilon)}{T} \right)^2 + \frac{\epsilon - \nu_n}{T} \frac{\partial \nu_n}{\partial T} - \frac{\Delta_n}{T} \frac{\partial \Delta_n}{\partial T} \right]. \quad (15)$$

At high enough density, as in the core of a neutron star, neutron pairs are very loosely bound so that $\Delta_n \ll \nu_n$. In the weak coupling approximation (Landau & Lifchitz 1980b), Eq. (10) is replaced by

$$1 \approx -\frac{1}{8} v^\pi(n_n) D(\nu_n) \int_{-\infty}^{\nu_n + \varepsilon_\Lambda} d\epsilon \frac{1}{E(\epsilon)} \tanh \left(\frac{E(\epsilon)}{2T} \right), \quad (16)$$

and Eq. (11) by $\nu_n \approx T_{Fn}$, where the Fermi temperature is defined by $T_{Fn} = \epsilon_n(k = k_{Fn})$, see e.g. Eq. (6), and where $k_{Fn} = (3\pi^2 n_n)^{1/3}$ denotes the Fermi wave number. Equation (16) can be further approximated by (Landau & Lifchitz 1980b)

$$\log \left(\frac{\Delta_n(0)}{\Delta_n(T)} \right) \approx \int_0^{+\infty} \frac{dx}{\sqrt{x^2 + u^2} (1 + \exp(\sqrt{x^2 + u^2}))}, \quad (17)$$

with $u = \Delta_n(T)/T$ and the integration has been extended to $\pm\infty$. In their seminal paper, Levenfish & Yakovlev (1994) have solved Eq. (17) to calculate the neutron heat capacity at densities relevant for neutron star cores, and fitted the numerical results with the following analytical expression:

$$C_V^n(n_n, T) = R_{00}(u) C_V^{n(nor)}(n_n, T), \quad (18)$$

where $C_V^{n(nor)}$ is the heat capacity of non-superfluid neutrons, which in the quantum regime of strongly degenerate neutrons, $T \ll T_{Fn}$, is approximately given by (Landau & Lifchitz 1980b)

$$C_V^{n(FG)}(n_n, T) = \frac{\hbar^2}{4m_n^*} n_n^{1/3} \left(\frac{\pi}{3} \right)^{2/3} T = \frac{\pi^2}{2} n_n \frac{T}{T_{Fn}}. \quad (19)$$

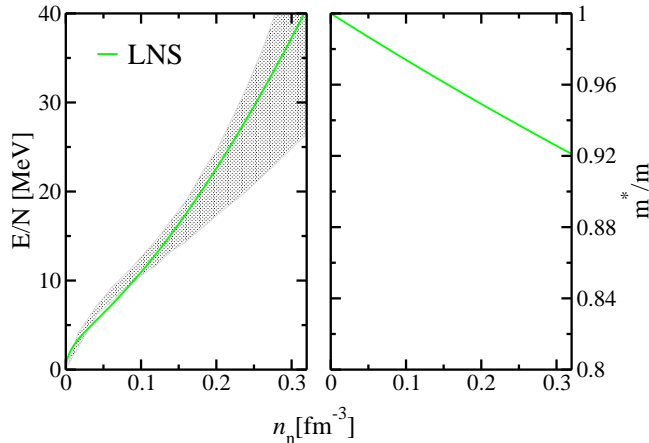


Figure 1. (Color online) Equation of state (left panel) and effective mass (right panel) in neutron matter for the LNS Skyrme functional (Cao et al. 2006). The grey area represents the range of equations of state obtained from quantum Monte Carlo calculations (Gandolfi et al. 2012). See text for details.

In Eq. (18), R_{00} is a correction factor introduced to account for the effects of superfluidity and was parametrized as (Levenfish & Yakovlev 1994)

$$R_{00}(u) = \left[a_0 + \sqrt{(a_1)^2 + (a_2 u)^2} \right]^\gamma \exp \left(b_0 - \sqrt{b_1^2 + u^2} \right), \quad (20)$$

where $u = \sqrt{1 - \tau} (c_0 - c_1/\sqrt{\tau} + c_2/\tau)$, $\tau = T/T_{sf}$.

Equations (18), (19), (20) have been widely applied in neutron-star cooling simulations. However, the weak-coupling approximation used to obtain these expressions may not be very accurate for the dilute neutron liquid that permeates the inner crust of a neutron star, especially in the shallowest region where Δ_n becomes comparable to ν_n . Note that in this case, the chemical potential ν_n may be very different from the Fermi energy. It was found, for instance, that the low density regime could be located in the BCS-BEC crossover, either close to the unitary limit, or, in some cases, almost entering the BEC regime (where the chemical potential becomes negative as $T \rightarrow 0$) (Margueron et al. 2007). The FTHFB equations (10)-(11) are however able to describe both the weak and the strong coupling regimes (Nozières & Schmitt-Rink 1985). For this reason, we have preferred to solve the set of coupled equations (10) and (11) without any further approximation instead of Eq. (17). The predictions for the heat capacity in the nonsuperfluid and superfluid phases will be discussed separately in Sections 3.1 and 3.2 respectively.

3.1 Nonsuperfluid phase: from the classical to the degenerate regimes

In this section, we first study the heat capacity of a non-superfluid neutron liquid. For this purpose, we have considered the LNS Skyrme functional (Cao et al. 2006), which was fitted to many-body calculations based on the Brueckner method and using realistic two- and three-body forces. In particular, the parameters of this functional were adjusted so as to reproduce both the equation of state and the effective mass in neutron matter as obtained from many-body calculations. As shown in Fig. 1, the equation of state given by this functional is in good agreement with more recent quantum Monte Carlo calculations (Gandolfi et al. 2012).

In Fig.2 (a), the neutron heat capacity calculated from Eq. (15) with $\Delta_n = 0$ is compared with the results obtained using the linear approximation (19). Large deviations can be observed in the low density region where $n_n \lesssim 10^{-3} \text{ fm}^{-3}$ or equivalently $\rho \lesssim 10^{12} \text{ g cm}^{-3}$ (see, e.g., Pearson et al. 2012). At high temperatures $T \gg T_{Fn}$, the heat capacity tends to the classical limit (Landau & Lifchitz 1980a)

$$C_V^{n(cl.)}(n_n) = \frac{3}{2} n_n. \quad (21)$$

In the ^3He normal phase, the coupling to phonons is known to largely correct Eq. (19) by the following term

$$\Delta C_V^{n(FG)}(n_n, T) = -\frac{3}{20} \pi^4 n_n B \left(\frac{T}{T_F} \right)^3 \log \frac{T}{T_c}, \quad (22)$$

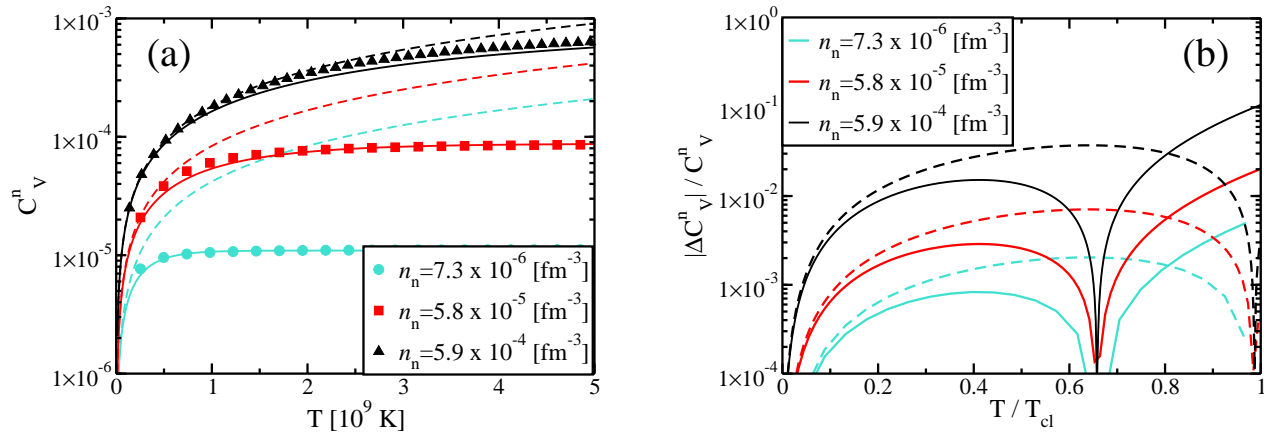


Figure 2. (Color online) On the left panel (a): heat capacity of nonsuperfluid neutrons as a function of temperature for different values of the density comparing the exact results (symbols) with the linear approximation given by Eq. (19) (dashed lines) and with the improved analytical formula given in Eq. (25) (solid lines). On the right panel (b): the correction to the heat capacity induced by the exchange of long-wavelength phonons: solid lines have been calculated using $x_c = 0.2$, while dashed with $x_c = 0.3$. See text for details.

where

$$B \approx -\frac{1}{2} \left[A_{0s}^2 \left(1 - \frac{\pi^2}{12} A_{0s} \right) + 3A_{0a}^2 \left(1 - \frac{\pi^2}{12} A_{0a} \right) \right] \quad (23)$$

and $A_{0s} = F_0/(1 + F_0)$ and $A_{0a} = G_0/(1 + G_0)$, F_0 (resp. G_0) being the density density (resp. spin-density spin-density) Landau parameter (Baym & Pethick 1991) and $T_c = x_c T_F$ is a cut-off temperature. Eq. (23) is the lowest order approximation considering only the monopolar contribution. Highest order contributions have been calculated by Pethick & Carneiro (1973). The correction $\Delta C_V^{n(FG)}$ normalized to $C_V^{n(FG)}$ is shown in Fig.2 (b) for the three densities (dashed-dotted lines) and for two different choices of the parameter x_c (see, e.g., Baym & Pethick 1991). This correction is shown up to the classical temperature T_{cl} since beyond this temperature, the system could not be treated with the same quantal approximation methods, and the limit is given by the classical expression (21). It is a negligible correction in the case of very diluted neutron matter (less than 1% in most of the cases). This is mainly due to the absolute value of the Landau Parameters F_0 and G_0 which are small compared to 1, for the considered densities.

In order to assess more precisely the validity of the linear approximation (19), we have calculated the relative deviation

$$\delta(T, n_n) = \frac{|C_V^n(T, n_n) - C_V^{n(FG)}(T, n_n)|}{C_V^n(T, n_n)}, \quad (24)$$

for the range of neutron densities encountered in neutron-star crusts (see, e.g., Pearson et al. 2012). Lines of constant δ in a temperature-density diagram are plotted in Fig. 3. Whereas δ is of the order of a few percents or less at the bottom of the neutron-star crust for temperatures $T \lesssim 10^{10}$ K, errors can be much larger in the shallower layers of the crust near the neutron-drip point where $n_n \rightarrow 0$.

The exact results for the neutron heat capacity can be represented by the following simple analytical expression

$$C_V^{n(FG-cl)}(n_n, T) \approx \frac{3}{2} n_n \left[1 - \exp\left(-\frac{T}{T_{cl}}\right) \right] \quad (25)$$

where $T_{cl} \equiv 3T_{Fn}/\pi^2$ is a characteristic temperature delimiting the classical and quantum regimes. This expression yields the correct asymptotic behaviours: at low temperatures ($T/T_{cl} \ll 1$) Eq.(25) reduces to Eq.(19), while at high temperatures ($T/T_{cl} \gg 1$), Eq.(25) tends to the classical limit (21). As shown in Fig. 2, Eq. (25) provides a very accurate interpolation between the low and high temperature limits. The classical temperature T_{cl} is also represented in Fig. 3, showing that at $T \approx T_{cl}$, the relative deviation $\delta(T, n_n)$ amounts to $\sim 30\%$.

Note that in Eq. (25), the effect of the neutron-neutron interactions are embedded in the neutron effective mass appearing in the expression of the Fermi temperature T_{Fn} . However, $m_n^* \approx m_n$ at densities below $n_n \sim 10^{-2} \text{ fm}^{-3}$ therefore the expression (25) is almost independent of the choice of the functional over this range of densities.

While in this paper, we are mostly interested in neutron matter, Eq. (25) can be easily adapted to evaluate the heat capacity of any other fermion species, e.g. electrons.

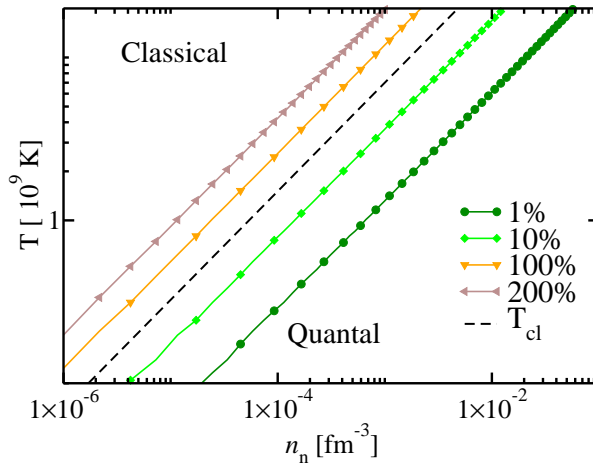


Figure 3. (Color online) Temperature as a function of density corresponding to fixed values of the error function $\delta(T, n_n)$. The dashed line represents the characteristic temperature T_{cl} appearing in Eq. (25) and delimiting the classical from the quantum regime. See text for details.

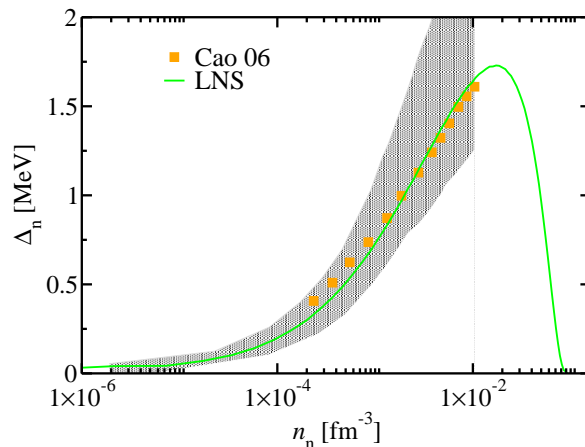


Figure 4. (Color online) 1S_0 neutron pairing gap as a function of density as obtained from Eq. (26) (solid line) and from (Cao et al. 2006) (symbols). The gray band is extracted from taking the most recent *ab-initio* results of Ref. (Gezerlis & Carlson 2010).

3.2 Superfluid phase

Let us now study the heat capacity in the superfluid regime and the transition to the normal phase at $T = T_{sf}$. In our calculations, we use an effective pairing interaction which is adjusted to mimic more microscopic interactions based on Brueckner method (Brueckner & Levinson 1955). We have adopted the ones obtained by Cao et al. (2006) which includes medium polarization effects beyond the mean-field. The reason for calibrating our effective pairing interaction to these results is that they were determined using the same Brueckner approach as the one we have used to fix the mean-field and the effective mass, see Section 3.1. In this way, the particle-hole and the particle-particle channels are consistently defined.

The microscopic pairing gaps calculated by Cao et al. (2006) at $T = 0$ can be conveniently parametrized by the following expression (Kaminker et al. 2001)

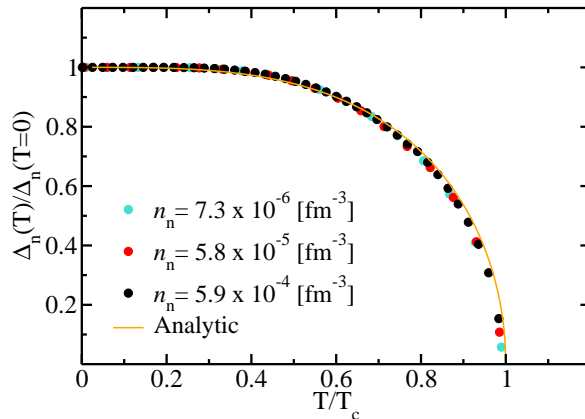
$$\Delta_n(T=0) = \Theta(k_{max} - k_{Fn}) \Delta_0 \frac{k_{Fn}^2}{k_{Fn}^2 + k_1^2} \frac{(k_{Fn} - k_2)^2}{(k_{Fn} - k_2)^2 + k_3^2}, \quad (26)$$

in which $\Theta(x)$ denotes the Heaviside unit step function. The values of the parameters Δ_0 , k_{max} , k_1 , k_2 , k_3 are given in Tab. 1. As shown in Fig. 4, expression (26) can well reproduce the gap by Cao et al. (2006).

In the literature several *ab-initio* calculations of the pairing gap have been performed (Gezerlis & Carlson 2010). They

Table 1. Values of the parameters entering into Eq. (26).

k_{max} [fm ⁻¹]	Δ_0 [MeV]	k_1 [fm ⁻¹]	k_2 [fm ⁻¹]	k_3 [fm ⁻¹]
1.37	3.37968	0.556092	1.38236	0.327517


Figure 5. (Color online) Evolution of the 1S_0 neutron pairing gap as a function of temperature for some representative value of the density of the system expressed in [fm⁻³]. The dots represent the exact FTHFB results, while the solid line is obtained using Eq. (27).

are included in the gray band in Fig.4. There are some discrepancies among them, as indicated by the thickness of the band, but the parametrization of the pairing gap that we consider (solid green line) remains within this band.

Injecting the gap expression (26) into the definition of the effective pairing force (8), we have solved the FTHFB Eqs. (1)-(2) and we have determined the evolution of the pairing gaps as a function of temperature. The value of the pairing cutoff can be arbitrarily chosen. As shown in Fig.5, the gap decreases with increasing temperature, and eventually vanishes at the critical temperature T_{sf} . The temperature dependence of the pairing gap can be accurately represented by the following expression (Goriely 1996)

$$\Delta_n(T) = \Delta_n(T=0) \sqrt{1 - \left(\frac{T}{T_{sf}}\right)^{3.23}} \Theta(T - T_{sf}), \quad (27)$$

for $T \leq T_{sf}$. The critical temperature can be obtained from the pairing gap at zero temperature from the well-known relation (Landau & Lifchitz 1980b)

$$T_{sf} = \frac{\exp(\xi)}{\pi} \Delta_n(T=0), \quad (28)$$

where $\xi \approx 0.577$ is the Euler-Mascheroni constant. Equations (26), (27) and (28) provide a convenient parametrization of the evolution of the pairing gaps as a function of both temperature and density.

From the solutions of the FTHFB Eqs. (1)-(2), we have calculated the heat capacity using Eq. (15) and compared the results with those obtained using the analytical formula proposed by Levenfish & Yakovlev (1994). As shown in Fig. 6, this formula reproduces very well the FTHFB results in all cases and for the domain of temperature ranging from 0 to few MeV.

The formula of Levenfish & Yakovlev (1994) can be further improved by readjusting the numerical parameters of the R_{00} form factor. As shown in Fig.6, the new formula for the heat capacity

$$C_V^n(n_n, T) \approx \frac{3}{2} n_n R_{00}(T) \left[1 - \exp\left(-\frac{T}{T_{cl}}\right) \right] \quad (29)$$

provides a very good fit to the exact FTHFB results both in the quantal and classical regimes.

4 CONCLUSIONS

The heat capacity of dilute neutron matter has been calculated in the framework of the finite-temperature Hartree-Fock-Bogoliubov method using an energy density functional fitted to microscopic calculations at zero temperature. Although the

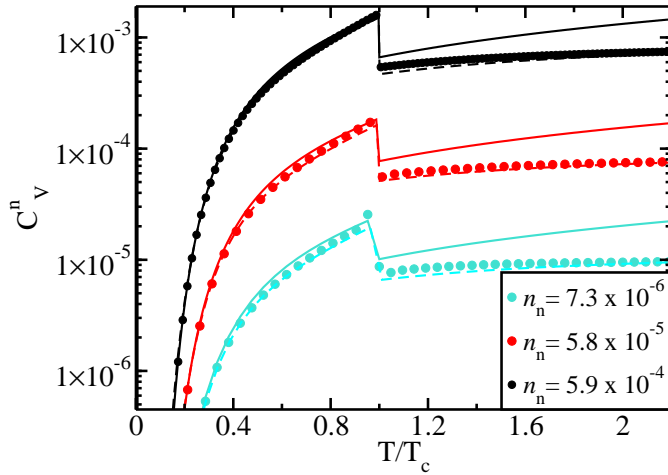


Figure 6. (Color online) Neutron heat capacity: FTHFB results (dots) are compared to the original expression Levenfish & Yakovlev (1994), see Eq.(18), (solid line) and to the new expression (25) with refitted parameters given in Tab.2 (dashed line). The values of the density are expressed in $[\text{fm}^{-3}]$.

	LY	present
a_0	0.4186	-0.7294
a_1	1.007	2.331
a_2	0.501	0.806
b_0	1.456	0.743
b_1	1.456	0.743
γ	2.5	2.5
c_0	1.456	-2.689
c_1	0.157	-3.800
c_2	1.764	0.826

Table 2. Values of the parameters appearing in Eq.(20). LY refers to the original values given by Levenfish & Yakovlev (1994).

heat capacity is found to be well reproduced by the empirical expressions of Levenfish & Yakovlev (1994) at high enough density, it differs substantially in the dilute limit corresponding to the shallow region of the inner crust of a neutron star. In particular, the use of Eq.(18) overestimates the heat capacity of nonsuperfluid neutrons, hence also the thermal relaxation time of neutron-star crusts. Indeed, nonsuperfluid neutrons provide the main contribution to the heat capacity of the neutron-star inner crust (Gnedin et al. 2001). We have proposed a new analytical expression obtained by combining Eqs. (18), (20), (25), that tends to the correct limits both at $T = 0$ and at $T \rightarrow +\infty$. This expression also takes into account the superfluid transition at $T = T_{sf}$, the critical temperature T_{sf} being given by Eqs. (26) and (28).

The presence of neutron-proton clusters in the inner crust of a neutron star may impact the heat capacity of the neutron liquid (Pizzochero et al. 2002; Sandulescu 2004; Monrozeau et al. 2007; Fortin et al. 2010; Chamel et al. 2010; Pastore 2012), an effect which we haven't considered in this study. While this approximation was shown to be very accurate in the normal phase (Chamel et al. 2009), it may induce larger errors in the superfluid phase. In most regions of the inner crust, the pairing gap hence also the critical temperature are reduced as compared to pure neutron matter calculations, but this effect can be easily included in the present expression for C_V^n by simply renormalizing T_{sf} (see, e.g., Chamel et al. 2010). As a matter of fact, this reduction of T_{sf} lies within the theoretical uncertainties of microscopic calculations in pure neutron matter. On the other hand, spatial inhomogeneities can drastically change the phase diagram of the neutron liquid near the neutron-drip transition (Margueron & Khan 2012; Pastore 2012). The effect of non-uniform matter could be parameterized as an additional correction to the uniform matter expressions, as performed by Fortin et al. (2010). The simple expression proposed

in this work, valid in all regimes from classical's to superfluid's ones, could efficiently be used to determine accurately the aforementioned corrections. Further studies are therefore needed to determine the neutron heat capacity in these layers of the star, but the present work provides an improved reference for more refined calculations taking into account the presence of nuclear clusters in the crust.

ACKNOWLEDGMENTS

This work was partially supported by the COST Action MP1304 and by the ANR SN2NS. N. C. acknowledges support from FNRS (Belgium). A.P. thanks M. Urban for the interesting comments that motivated this work.

REFERENCES

- Baldo M., Burgio G., 2012, Reports on Progress in Physics, 75, 026301
Baym G., Pethick C., 1991, Landau Fermi-liquid theory: concepts and applications. John Wiley & Sons
Bender M., Heenen P.-H., Reinhard P.-G., 2003, Reviews of Modern Physics, 75, 121
Brueckner K., Levinson C., 1955, Physical Review, 97, 1344
Cao L.-G., Lombardo U., Schuck P., 2006, Physical Review C, 74, 64301
Cao L. G., Lombardo U., Shen C. W., Giai N. V., 2006, Phys. Rev. C, 73, 014313
Chamel N., 2010, Physical Review C, 82, 014313
Chamel N., Goriely S., Pearson J. M., Onsi M., 2010, Physical Review C, 81, 045804
Chamel N., Haensel P., 2008, Living Rev. Relativity, 11, 10
Chamel N., Margueron J., Khan E., 2009, Physical Review C, 79, 012801(R)
Fantina A. F., Chamel N., Pearson J. M., Goriely S., 2012, Journal of Physics Conference Series, 342, 012003
Fortin M., Grill F., Margueron J., Page D., Sandulescu N., 2010, Physical Review C, 82, 065804
Gandolfi S., Carlson J., Reddy S., 2012, Phys. Rev. C, 85, 032801
Gezerlis A., Carlson J., 2010, Phys. Rev. C, 81, 025803
Gnedin O. Y., Yakovlev D. G., Potekhin A. Y., 2001, MNRAS, 324, 725
Goodman A. L., 1981, Nuclear Physics A, 352, 30
Goriely S., 1996, Nuclear Physics A, 605, 28
Haensel P., Potekhin A. Y., Yakovlev D. G., 2007, Neutron Stars I. Vol. 3, Springer
Kaminker A., Haensel P., Yakovlev D., 2001, arXiv preprint astro-ph/0105047
Landau L. D., Lifchitz E. M., 1980a, Statistical Physics, Part 1. Pergamon Press
Landau L. D., Lifchitz E. M., 1980b, Statistical Physics, Part 2. Pergamon Press
Lattimer J. M., Van Riper K. A., Prakash M., Prakash M., 1994, The Astrophysical Journal, 425, 802
Levenfish K. P., Yakovlev D. G., 1994, Astronomy Reports, 38, 247
Margueron J., Khan E., 2012, Physical Review C, 86, 065801
Margueron J., Sagawa H., Hagino K., 2007, Physical Review C, 76, 064316
Margueron J., Sandulescu N., 2012, in Bertulani C. A., Piekarewicz J., eds, , Neutron Star crust. World Scientific, pp 68–86
Monrozeau C., Margueron J., Sandulescu N., 2007, Physical Review C, 75, 065807
Nozières P., Schmitt-Rink J., 1985, Journal of Low Temperature Physics, 59, 195
Page D., Reddy S., 2012, Neutron Star crust. edited by C. Bertulani and J. Piekarewicz, Nova Science Publishers (2012), pp.281-308
Pastore A., 2012, Physical Review C, 86, 065802
Pearson J., Chamel N., Goriely S., Ducoin C., 2012, Physical Review C, 85, 065803
Pethick C. J., Carneiro G. M., 1973, Physical Review A, 7, 304
Pizzochero P. M., Barranco F., Vigezzi E., Broglia R. A., 2002, The Astrophysical Journal, 569, 381
Sandulescu N., 2004, Physical Review C, 70, 025801
Skyrme T. H. R., 1958, Nuclear Physics, 9, 635